Suppression of ionization probability due to Rabi oscillations in the resonance two-photon ionization of He by EUV free-electron lasers

Tokuei Sako,[1,*] Junichi Adachi,[2,3] Akira Yagishita,[2,3,†] Makina Yabashi,[3] Takashi Tanaka,[3] Mitsuru Nagasono,[3] and Tetsuya Ishikawa[3]

[1]*Laboratory of Physics, College of Science and Technology, Nihon University, 7-24-1 Narashinodai, Funabashi, Chiba 274-8501, Japan*

[2]*Photon Factory, Institute of Materials Structure Science, KEK, 1-1 Oho, Tsukuba, Ibaraki 305-0801, Japan*

[3]*RIKEN, SPring-8 Center, Sayo, Hyogo 679-5148, Japan*

(Received 29 August 2011; published 16 November 2011)

The two-photon resonance ionization probability of atoms in strong extreme-ultraviolet free-electron laser (EUV FEL) pulses has been investigated by the model of time-dependent wave packet propagation of a light-coupled multilevel atom. Under the simulation within the model assuming single-mode FEL pulses, the ionization probability $P_{\rm ion}$ has shown characteristic dependences on the scaled coupling parameter U_{gi} between two levels of the ground (g) and intermediate (i) resonance states, namely, $P_{\rm ion} \propto (U_{gi})^n$, with n being equal to $\sim$2, less than 1, and $\sim$1 for the small, medium, and large U_{gi} regimes, respectively. This power dependence of the ionization probability has been interpreted due to Rabi oscillations between g and i states. To compare with recent experimental results on the same condition, the multimode nature of self-amplitude spontaneous emission (SASE) FEL pulses has been managed in the simulation. Then, the recent experimental laser-power dependence of the two-photon resonance ionization of He [Sato *et al.*, J. Phys. B **44**, 161001 (2011)] has been well described by that for the large U_{gi} regime of the simulation, i.e., $n \sim 1$. Thus, the observed linear laser-power dependence has been rationalized as being caused by the strong Rabi oscillations between the $(2p)$–$(1s)$ states.

DOI: 10.1103/PhysRevA.84.053419 PACS number(s): 32.80.Rm, 82.53.Kp, 32.80.Fb

I. INTRODUCTION

The new tunable extreme-ultraviolet free-electron laser (EUV FEL) from the Spring-8 Compact SASE Source (SCSS) [1,2] has provided a new opportunity to investigate fundamental quantum phenomena, i.e., the interaction between a two-level atom and high-intensity, high-frequency radiation. Suppose that one tunes the laser frequency of a light pulse of roughly 100-fs duration to a transition frequency of the atom. A photon in the pulse brings the atom from the ground state to its excited state, and then the atom in the excited sate in the strong light field emits a photon with the same phase and frequency as the laser light. This cycling process of absorbing and emitting photons is called Rabi oscillations [3]. During the cycle the time-dependent quantum state of the atom coupled with the light field is usually in a superposition of [(ground state) + $(N+1)$ photons] and [(excited state) + N photons]. The oscillating coupled system can be ionized by absorbing one more photon in the same light pulse. As a result, the end of the light pulse probes the oscillating system. Thus, such a resonance two-photon ionization process is completely different from the *sequential nonresonance* ionization, which has been studied in recent years by high-intensity FEL lights [4–8]. The ionization probability of such nonresonance multiphoton processes is well described by lowest-order perturbation theory, i.e., according to the theory, expected to be valid at the laser intensity $I < 10^{15}$ W/cm^2; the ionization probability $P_{\rm ion}$ should increase with I as $P_{\rm ion} = \sigma_n \times I^n$, where σ_n is the generalized n-photon cross section and n is the number of photons needed for ionization [9]. On the other hand, the ionization probability of high-intensity resonance multiphoton ionization would have a different dependence on I because of Rabi oscillations between the ground and intermediate resonance states, as early theoretical studies indicated their importance [10,11].

Recently, pioneering experimental reports on resonance multiphoton ionization of atoms by strong EUV FEL lights have appeared [12–16]. Among these studies Miyauchi *et al.* [14] and Sato *et al.* [16] have revealed that the ionization probability deviates strongly from the conventional I^n scaling for nonresonance multiphoton ionization. We note here that a deviation from the I^n scaling law was also reported long ago in the multiphoton ionization of atoms by visible and infrared lasers [11,17]. (See also a review by Burnett *et al.* [18] for the suppression of ionization of atoms by nonperturbative light-atom interaction beyond the multiphoton regime.) To understand the observed nonperturbative laser-power dependence in the high-frequency regime of EUV FEL, we have performed in the present study a numerical simulation of the time-dependent ionization probability by solving the time-dependent Schrödinger equation for a light-coupled three-level atom modeling the resonance two-photon ionization of atoms, assuming single-mode FEL pulses. A nonperturbative time-independent approach such as the Floquet approach [19–23] may also be used to rationalize the deviation from the power law, but it is not suitable for describing nonstational dynamical Rabi oscillations that occur within short laser pulses.

Furthermore, the multimode nature of the EUV FEL pulses has been taken into account in our simulation, and its effect on the ionization probability has been examined. The result has rationalized the strong deviation from the I^2 scaling for the ionization probability of the resonance two-photon process of He atom, which has been reported very recently by Sato *et al.* [16]. More importantly, we have found that the Rabi oscillation during the course of single-light-pulse

*sako@phys.ge.cst.nihon-u.ac.jp
†akira.yagishita@kek.jp

duration plays the essential role in determining the resonance two-photon ionization probability.

II. THEORETICAL MODEL AND COMPUTATIONAL DETAILS

The excitation scheme of the present theoretical model, i.e., the two-photon resonance ionization of a model atom, which is schematically illustrated in Fig. 1, is as follows: The target atom in its ground state (denoted by $|g\rangle$) is resonantly excited to an intermediate state $|i\rangle$ by absorbing one photon whose energy $\hbar\omega$ coincides with the energy difference between $|i\rangle$ and $|g\rangle$ [step (a)]. Then, the excited atom in $|i\rangle$ undergoes two distinct processes; (i) returning to $|g\rangle$ by emitting the same photon [step (b)] or (ii) being ionized to a virtual state $|v\rangle$ in the ionization continuum by absorbing another photon with the same energy [step (c)]. These three transition processes induced by photons occur simultaneously as far as the relevant levels are populated. Our theoretical model describing this scheme thus consists of the three levels $|g\rangle$, $|i\rangle$, and $|v\rangle$.

The general time-dependent Schrödinger equation for a nonrelativistic N-electron atom coupled with a classical electromagnetic field is given in atomic units as

$$i\frac{\partial}{\partial t}\Psi = \left[\sum_{k=1}^{N}\frac{1}{2}\{-i\vec{\nabla}_k + \vec{A}(\vec{r}_k,t)\}^2 - \sum_{k=1}^{N}\frac{Z}{|\vec{r}_k|} + \sum_{k>l}^{N}\frac{1}{|\vec{r}_k-\vec{r}_l|}\right]\Psi, \tag{1}$$

where $\{\vec{r}_k\}$ $(k = 1, \ldots, N)$, Z, and $\vec{A}(\vec{r}_k,t)$ represent, respectively, the spatial coordinates for the kth electron, the nuclear charge, and the vector potential at the position of the kth electron and time t. In Eq. (1) the position of the nucleus is fixed at the origin. There are a number of practical ways for transforming this equation into a particular form suitable for actual calculation thanks to the gauge invariance of expectation values of observables under any unitary transformations. Among others, the so-called length gauge has been adopted in the present study. This is because (i) the dipole approximation, that is, neglecting the position dependence of the vector potential, such that $\vec{A}(\vec{r}_k,t) \cong \vec{A}(t)$, is valid for the present EUV FEL whose wavelength of ~58 nm is still much larger than a typical atomic size of ~0.1 nm and (ii) the transformed Hamiltonian becomes a simple sum of the field-free atomic Hamiltonian and a dipole interaction term in this representation, as shown by Eq. (2). By applying the unitary transformation of $\prod_{k=1}^{N}\exp[i\vec{A}(t)\cdot\vec{r}_k]$ to the wave function Ψ on both sides of Eq. (1) and then introducing the electric field vector of $\vec{E}(t) = -\frac{\partial}{\partial t}\vec{A}(t)$, the time-dependent Schrödinger equation for the transformed wave function $\tilde{\Psi}$ becomes

$$i\frac{\partial}{\partial t}\tilde{\Psi} = \left[\hat{H}_0 + \vec{E}(t)\cdot\sum_{k=1}^{N}\vec{r}_k\right]\tilde{\Psi}, \tag{2}$$

where $\hat{H}_0$ on the right-hand side of Eq. (2) represents the field-free atomic Hamiltonian, which is given explicitly as

$$\hat{H}_0 \equiv -\sum_{k=1}^{N}\frac{1}{2}\vec{\nabla}_k^2 - \sum_{k=1}^{N}\frac{Z}{|\vec{r}_k|} + \sum_{k>l}^{N}\frac{1}{|\vec{r}_k-\vec{r}_l|}. \tag{3}$$

The atomic unit of electric field strength is the field felt by an electron in the ground state of atomic hydrogen, $E_a = 5.14\times10^9$ V/cm, and the corresponding intensity is $I_a = 3.51\times10^{16}$ W/cm^2.

By relying on the resonance conditions, i.e., $\hbar\omega = \varepsilon_i - \varepsilon_g = \varepsilon_v - \varepsilon_i$, where $\{\varepsilon_\alpha\}$ $(\alpha = g,i,v)$ denote the eigenenergies of the respective states (i, g, and v), the time-dependent wave function $\tilde{\Psi}$ can be expanded in terms of these three field-free states as

$$\tilde{\Psi}(t) = \sum_{\alpha=\{g,i,v\}} c_\alpha(t)|\alpha\rangle. \tag{4}$$

Since $|v\rangle$, $|i\rangle$, and $|v\rangle$ are the eigenstates of the field-free Hamiltonian $\hat{H}_0$, they satisfy the following eigenvalue

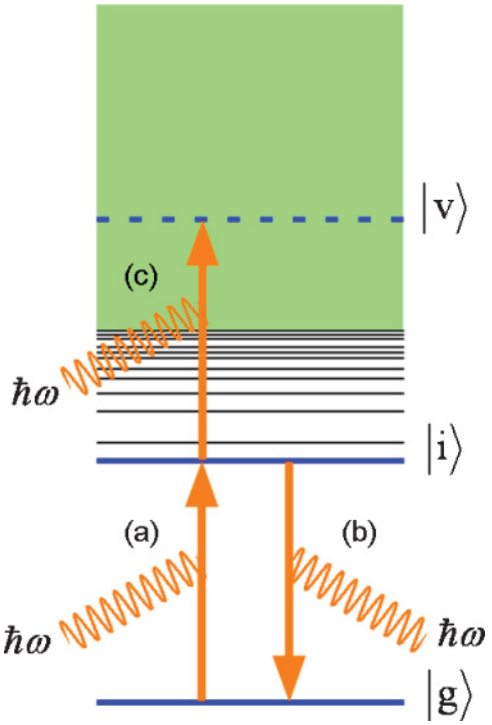

FIG. 1. (Color online) A schematic illustration of the excitation scheme in the present multilevel atom modeling the resonance two-photon ionization of He. The three transition processes, (a)–(c), induced by photons with energy $\hbar\omega$ are indicated by orange (light gray) arrows. The solid blue (dark gray) bars, $|g\rangle$ and $|i\rangle$, represent the ground and intermediate resonance states, respectively, while the dotted one, $|v\rangle$, represents the virtual state above the ionization threshold that decays into the ionization continuum indicated by the light green (light gray) area.

equations:

$$\hat{H}_0|\alpha\rangle = \varepsilon_\alpha|\alpha\rangle, \quad (\alpha = g, i), \tag{5}$$

$$\hat{H}_0|v\rangle = (\varepsilon_v - i\gamma)|v\rangle. \tag{6}$$

As shown in Eq. (6), the imaginary part of the eigenenergy $-i\gamma$ is introduced for the virtual state $|v\rangle$ so that the probability density for this state decays automatically into the ionization continuum. By inserting (4) into the time-dependent Schrödinger equation (2), the differential equation for the expansion coefficients $\{c_\alpha(t)\}$ $(\alpha = g, i, v)$ is derived as

$$i\frac{d}{dt}\begin{pmatrix} c_g(t) \\ c_i(t) \\ c_v(t) \end{pmatrix} = \begin{pmatrix} \varepsilon_g & \vec{E}(t)\cdot\langle g|\sum_{k=1}^{N}\vec{r}_k|i\rangle & 0 \\ \vec{E}(t)\cdot\langle i|\sum_{k=1}^{N}\vec{r}_k|g\rangle & \varepsilon_{\rm i} & \vec{E}(t)\cdot\langle i|\sum_{k=1}^{N}\vec{r}_k|v\rangle \\ 0 & \vec{E}(t)\cdot\langle v|\sum_{k=1}^{N}\vec{r}_k|i\rangle & \varepsilon_v - i\gamma \end{pmatrix}\begin{pmatrix} c_g(t) \\ c_i(t) \\ c_v(t) \end{pmatrix}. \tag{7}$$

Assuming that the laser field is linearly polarized along the z axis, the off-diagonal matrix elements in Eq. (7) can be simplified such that

$$\vec{E}(t)\cdot\langle\alpha|\sum_{k=1}^{N}\vec{r}_k|\beta\rangle = E(t)T_{\alpha\beta}, \quad (\{\alpha,\beta\} = \{g, i, v\}), \tag{8}$$

where $E(t)$ and $T_{\alpha\beta}$ represent the time-dependent electric field along the polarization direction and the transition dipole matrix elements along this polarization direction, respectively.

The differential equation (7) for the expansion coefficients can be integrated by a standard computational technique, such as a split operator method [24] or a higher-order symplectic integrator method [25]. The procedure can be briefly outlined as follows: The matrix on the right-hand side of Eq. (7) is split into a sum of two matrices **A** and **B**, where

$$\mathbf{A} \equiv \begin{pmatrix} \varepsilon_g & E(t)T_{gi} & 0 \\ E(t)T_{ig} & \varepsilon_i & E(t)T_{iv} \\ 0 & E(t)T_{vi} & \varepsilon_v \end{pmatrix}, \tag{9}$$

and

$$\mathbf{B} = \begin{pmatrix} 0 & 0 & 0 \\ 0 & 0 & 0 \\ 0 & 0 & -i\gamma \end{pmatrix}. \tag{10}$$

Then, Eq. (7) can be integrated for an infinitesimal time step Δt as

$$\begin{pmatrix} c_g(t+\Delta t) \\ c_i(t+\Delta t) \\ c_v(t+\Delta t) \end{pmatrix} \cong \exp(-i\,\Delta t\mathbf{B}/2)\exp(-i\,\Delta t\mathbf{A}) \times \exp(-i\,\Delta t\mathbf{B}/2)\begin{pmatrix} c_g(t) \\ c_i(t) \\ c_v(t) \end{pmatrix}. \tag{11}$$

The two exponential functions, $\exp(-i\,\Delta t\mathbf{B}/2)$ and $\exp(-i\,\Delta t\mathbf{A})$, involving a matrix as its argument are evaluated as

$$\exp(-i\,\Delta t\mathbf{B}/2) = \begin{pmatrix} 0 & 0 & 0 \\ 0 & 0 & 0 \\ 0 & 0 & \exp(-\gamma\,\Delta t/2) \end{pmatrix} \tag{12}$$

and

$$\exp(-i\,\Delta t\mathbf{A}) = \mathbf{C}\mathbf{C}^{-1}\exp(-i\,\Delta t\mathbf{A})\mathbf{C}\mathbf{C}^{-1} = \mathbf{C}\begin{pmatrix} \exp(-i\,\Delta t\alpha_1) & 0 & 0 \\ 0 & \exp(-i\,\Delta t\alpha_2) & 0 \\ 0 & 0 & \exp(-i\,\Delta t\alpha_3) \end{pmatrix}\mathbf{C}^{-1}, \tag{13}$$

respectively, where **C** is a matrix that diagonalizes **A** such that

$$\mathbf{C}^{-1}\mathbf{A}\mathbf{C} = \begin{pmatrix} \alpha_1 & 0 & 0 \\ 0 & \alpha_2 & 0 \\ 0 & 0 & \alpha_3 \end{pmatrix}. \tag{14}$$

Repeating the procedure defined by Eq. (11) gives the time-dependent coefficients $\{c_\alpha(t)\}$ $(\alpha = g, i, v)$ at any desired time t. The resultant $\{c_\alpha(t)\}$ $(\alpha = g, i,$ and $v)$ give the survival probability of the atom under the laser pulse as $\rho(t) = |c_g(t)|^2 + |c_i(t)|^2 + |c_v(t)|^2$ with $\rho(0) = 1$. The time-dependent ionization probability is then calculated as $P_{\rm ion}(t) = 1 - \rho(t)$, which represents the proportion of atoms ionized during the time $0 \sim t$. Because of the exponential decay factor $\exp(-\gamma\,\Delta t/2)$ that appears in Eq. (12) the probability density at $|v\rangle$, $|c_v(t)|^2$, decays into the ionization continuum promptly, and thus it is negligibly small throughout the simulation. It is noted that the value of this γ parameter can be chosen arbitrarily but should be large enough so as to prohibit an unphysical backward transition from $|v\rangle$ to $|i\rangle$. Thanks to this population decay through $|v\rangle$, $\rho(t)$ decreases as the time proceeds. After the electric field of the laser pulse diminishes to practically zero, the survival probability ρ and the ionization probability $P_{\rm ion}$ remain unchanged.

The laser intensity I is determined experimentally from the energy per laser pulse that is divided by the focal spot size and a pulse duration, i.e., the FWHM pulse width $T_{\rm FWHM}$. Then, the time-dependent electric field $E(t)$ of the laser pulse in Eq. (8) is related to the laser intensity I as follows in atomic units:

$$I = \frac{1}{T_{\rm FWHM}} \int_{-\infty}^{\infty} dt |E(t)|^2. \tag{15}$$

From Eqs. (8) and (15), a useful parameter concerning the ionization probability may be defined such that

$$U_{gi} = I|T_{gi}|^2. \tag{16}$$

This U_{gi} parameter controls the transition strength between $|g\rangle$ and $|i\rangle$, i.e., processes (a) and (b) in Fig. 1. Although the ionization probability depends on a similar parameter U_{iv} as well, which controls the excitation from $|i\rangle$ to $|v\rangle$, the transition probability for this process [(c) in Fig. 1] depends simply on I linearly thanks to the no-return process from $|v\rangle$ to $|i\rangle$. Since the absolute value of the ionization probability is not discussed in the present study, we arbitrarily set, for example, $U_{iv} = 0.01U_{gi}$. Atomic units are used throughout the simulation.

III. RESULTS AND DISCUSSION

A. Two-photon resonance ionization by a single-mode Gaussian pulse

In Fig. 2, the ionization probability obtained from the simulation, modeling the resonance two-photon single ionization of the He atom by a Gaussian laser pulse of $E(t)$ with $T_{\rm FWHM} = 4134$ (100 fs) and with $\hbar\omega = \varepsilon_i - \varepsilon_g = \varepsilon_v - \varepsilon_i = 0.780$ (21.2 eV), is plotted as a function of the U_{gi} parameter. Figure 2 shows that for sufficiently small values of U_{gi} (e.g., $U_{gi} \sim 1 \times 10^{-8}$) the ionization probability behaves as a straight line with slope 2.0 in the log-log plot. This clearly indicates that the ionization probability persists to the

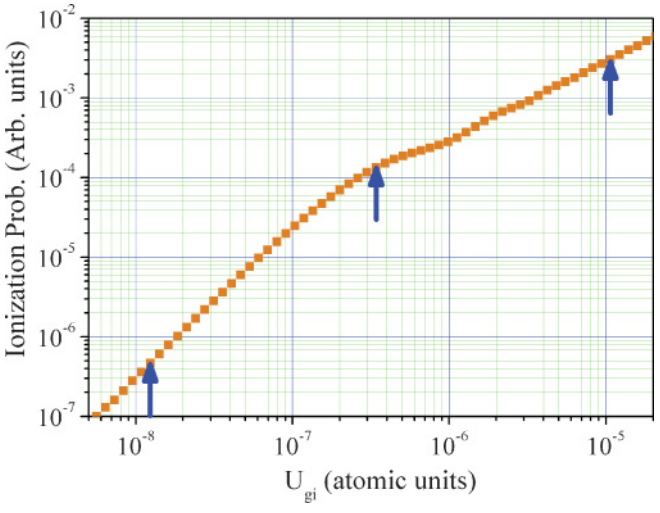

FIG. 2. (Color online) The ionization probability of the multilevel atom of the present study under a single-mode Gaussian laser pulse of 100-fs duration for different U_{gi}. The three blue (dark gray) arrows indicate the results for $U_{gi} = 1.4 \times 10^{-8}$, 3.4×10^{-7}, and 1.1×10^{-5}, corresponding to a typical value in the large, medium, and small regimes of $U_{\rm gi}$, respectively.

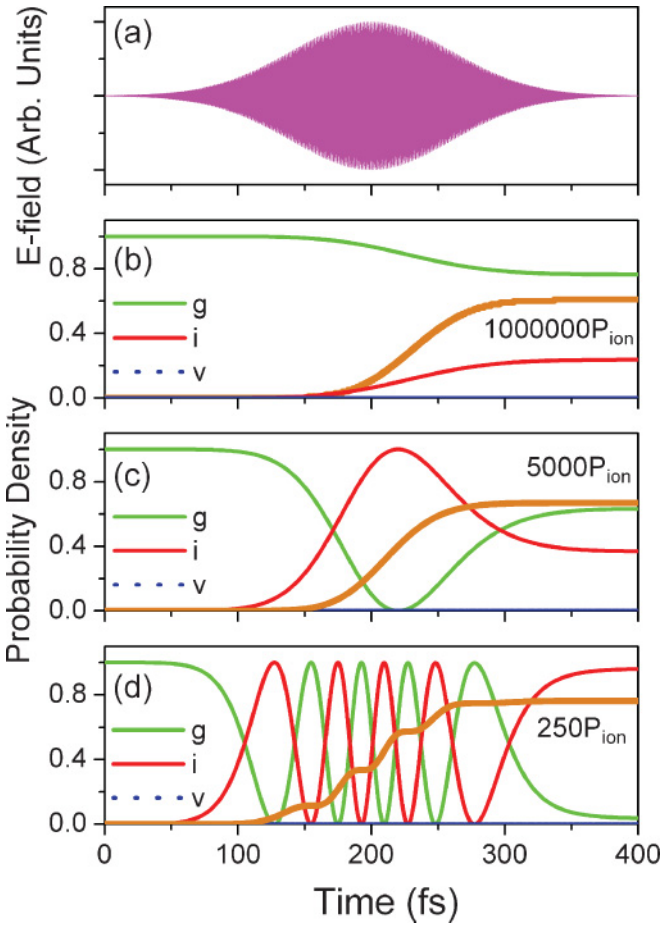

FIG. 3. (Color online) The time evolution (a) of the electric field of the laser pulse and of the probability densities among the three levels for different U_{gi}: (b) 1.4×10^{-8}, (c) 3.4×10^{-7}, and (d) 1.1×10^{-5}. The solid green (solid light gray), red (solid dark gray), and dashed blue (dashed dark gray) curves represent the densities for the ground state $|g\rangle$, the intermediate resonance state $|i\rangle$, and the virtual state $|v\rangle$, respectively. The density for $|v\rangle$ is negligibly small throughout the simulation and is superimposed on the x axis (see text). The thick orange (thick light gray) curve represents the ionization probability $P_{\rm ion}$ magnified by a numeral factor indicated in each plot.

I^2 power law even for the resonance case in this small U_{gi} range. However, when U_{gi} exceeds 2×10^{-7}, the ionization probability starts to deviate downward from this straight line and follows a nonmonotonous curve whose average slope is less than 1.0. When U_{gi} increases further, the ionization curve converges to a straight line with slope 1.0, as seen in Fig. 2.

In order to clarify the origin of this strong deviation from the I^2 power law, the time evolution of the probability distribution among the three levels, i.e., $|c_\alpha(t)|^2$ ($\alpha = g, i$, and v), is examined and plotted in Fig. 3 for $U_{gi} = 1.4 \times 10^{-8}$, 3.4×10^{-7}, and 1.1×10^{-5}. In Fig. 3, the alternating electric field of the laser pulse is shown in Fig. 3(a). Figure 3(b) ($U_{gi} = 1.4 \times 10^{-8}$), in a weak-field regime, shows that the probability in the ground state $|c_g(t)|^2$ indicated by the solid green (light gray) curve starts to decrease from unity at around $t = 150$ fs, when the amplitude of the laser pulse rises close to its peak. Synchronizing with the decrease in $|c_g(t)|^2$, the probability in the intermediate state $|c_i(t)|^2$ [solid red (dark

gray) curve] as well as the ionization probability $P_{\rm ion}(t)$ (thick orange curve) appears and increases until around $t = 300$ fs, when the laser field becomes so small it is unable to ionize the atom further. Figure 3(c) ($U_{gi} = 3.4 \times 10^{-7}$), at the beginning of the deviation from the straight line, shows that $|c_g(t)|^2$ decreases sharply after passing through $t = 150$ fs and becomes zero at $t = 222$ fs. Synchronizing with this decrease in $|c_g(t)|^2$, the probability in the intermediate state $|c_i(t)|^2$ increases sharply and becomes almost unity at the same time, when $|c_g(t)|^2$ becomes zero. Then, in turn, $|c_g(t)|^2$ increases and $|c_i(t)|^2$ decreases. This is a clear indication of the beginning of a Rabi oscillation between the ground and intermediate states. Since the laser pulse is not long enough with respect to the period of the Rabi oscillation in this regime, $|c_g(t)|^2$ and $|c_i(t)|^2$ converge to a constant value before completing their latter half cycle of oscillation. Therefore, since the ionization proceeds via $|i\rangle$, the decrease of the probability being in the i state prohibits efficient ionization. It is noted that if the probability $|c_i(t)|^2$ were increasing monotonously after the peak time of $t = 222$ fs, the ionization probability would increase further as well and would follow the prediction by the I^2 power law. As can be seen in Fig. 2, however, the ionization probability becomes smaller than the prediction from the lowest-order perturbation theory when Rabi oscillations take place.

This suppression of ionization probability due to the Rabi oscillations is evidently revealed in the result for $U_{gi} = 1.1 \times 10^{-5}$ displayed in Fig. 3(d). As indicated by the third arrow in Fig. 2, this value of 1.1×10^{-5} for the interaction strength U_{gi} deeply penetrates into the regime, where the laser-intensity dependence of the ionization probability deviates significantly from the I^2 power law and exhibits being almost linear with respect to I. The time evolution of the probabilities for the g and i states clearly manifests the Rabi oscillations of four and a half cycles. The ionization probability $P_{\rm ion}(t)$ increases step by step, passing the rising edge of the probability for the intermediate i state, $|c_i(t)|^2$, and staying almost unchanged during the period of time when $|c_i(t)|^2$ decreases to zero due to the second half cycle of Rabi oscillation. When the interaction strength U_{gi}, or, equivalently, the laser intensity I, becomes larger, the number of cycles for the Rabi oscillations in the laser pulse increases. In the further inspection of Fig. 3(d), it should be noticed that the number of decreasing edges in $|c_i(t)|^2$ is the same as that of the rising edge. Reflecting this, the cycle averages of the probability densities for the i and g states become almost equal to each other; that is, the survival probability is equally shared by the i and g states. As a result, the probability density for the i state becomes independent of the value of U_{gi} in this large U_{gi} regime. Then, the ionization probability depends only on the one-way excitation from $|i\rangle$ to $|v\rangle$ [process (c) in Fig. 1], giving a linear dependence on I.

B. Multimode effects

It may be noted that the EUV FEL pulses generated from the SCSS are not ideal single-mode Gaussian pulses but are multimode in nature [1,2]. Therefore, the results of numerical simulations obtained in the previous section assuming a single-mode laser pulse are not directly compared with the relevant experimental data. Therefore we have performed further numerical simulations using numerical data for self-amplitude spontaneous emission (SASE) FEL pulses for $E(t)$.

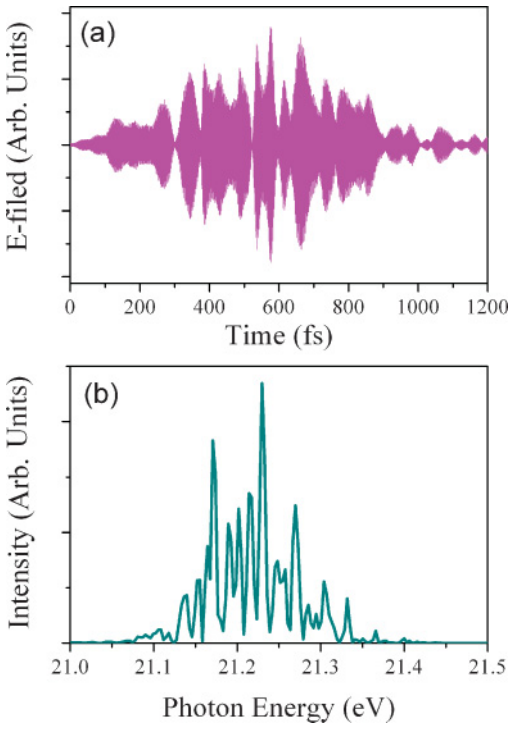

FIG. 4. (Color online) (a) An example of the FEL pulses employed in the simulation and (b) its energy-domain spectrum.

An example of the EUV FEL pulse obtained from the simulation code SIMPLEX [26] is presented in Fig. 4 for both time and energy domains. The time-domain FEL pulse displayed in Fig. 4(a) is largely different from the single-mode Gaussian pulse displayed in Fig. 3(a) in that it has a complicated structure due to interferences between different energy components, as evidenced by Fig. 4(b). In actually obtainable FEL pulses, there also exist some random fluctuations in the energy spectrum of Fig. 4(b) [1,2]. That is, the shot-by-shot FEL pulses are not identical to each other in the time domain as well as in the energy domain. Therefore, first for a set of ten FEL pulses, we have performed individually simulations by putting a set of ten time-dependent electric fields, one of which is shown in Fig. 4(a), into $E(t)$ in Eq. (7). A definition of the pulse width $T_{\rm FWHM}$ for the FEL pulses is not trivial owing to their complicated interference pattern, as shown in Fig. 4(a). On the one hand, in the experiment on the He atom, with which we compare our simulation results in the next section, the laser intensity was estimated by assuming $T_{\rm FWHM} = 300$ fs [16]. Therefore, we have also adopted $T_{\rm FWHM} = 300$ fs for consistency in our definition of laser intensity in Eq. (15). Second, the individual results of the ionization probabilities for the set of ten FEL pulses were averaged to give a representative ionization curve as a function of U_{gi}. Finally, this averaged curve as a function of U_{gi} was transformed in the curve as a function of laser intensity I by the substitution of the absolute value of transition dipole moment matrix element into T_{gi} in Eq. (16). This enables us to compare the theoretical results with the experimental ones in the scale of the laser intensity I.

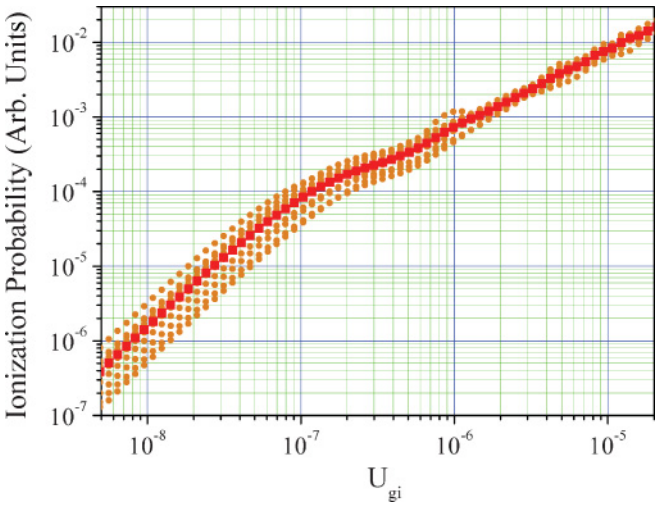

FIG. 5. (Color online) The ionization probability of the multilevel atom of the present study under the FEL pulses for different U_{gi}. The small orange (light gray) circles represent the results for each of the ten shots of the FEL pulses. The red (dark gray) squares represent their average.

Figure 5 represents the calculated ionization probabilities for each of the ten FEL pulses (small orange circles) and their averages (red squares). The red squares in Fig. 5, representing the averaged ionization curve, show similar characteristics as observed for the single Gaussian pulse; namely, the slope is $\sim$2 for the small U_{gi} regime and $\sim$1 for the large U_{gi} regime. It may be noted that the region of the curve with a slope less than 1.0 in the medium U_{gi} regime, which is seen for the result of a single-mode Gaussian pulse, is less visible for the averaged ionization curve of the FEL pulses. This is caused by an averaging procedure over the results of the fluctuating ionization probabilities for the individual FEL pulses, which blurs the fine details.

The time evolution of the probability densities among the three levels g, i, and v is plotted in Fig. 6 for the result obtained using the FEL pulse represented in Fig. 4(a). The U_{gi} parameters chosen for display are $U_{gi} = 1.1 \times 10^{-8}$, 3.0×10^{-7}, and 1.1×10^{-5}, which correspond to typical values in the small, medium, and large regimes, respectively. As shown in Figs. 6(b)–6(d), the ionization probability and the probability densities for the g and i states are spiky, not smooth, curves, although the overall trends are similar to those of the corresponding results for the single-mode Gaussian pulse. These spiky curves may be the reflection of the spiky pulse of Fig. 6(a), which is caused by modulations of the central frequency of the FEL pulse by other near-lying frequency components, as seen in Fig. 4(b). These modulations could accelerate or decelerate ionization probability every moment by modifying the amplitude of the time-dependent electric field, leading thus to fluctuations in the time-dependent ionization probability.

C. Application to the two-photon resonance ionization of He

The averaged ionization probability curve using the SASE FEL pulses obtained in the previous section, which is displayed in Fig. 5, is now compared with the experimental laser-

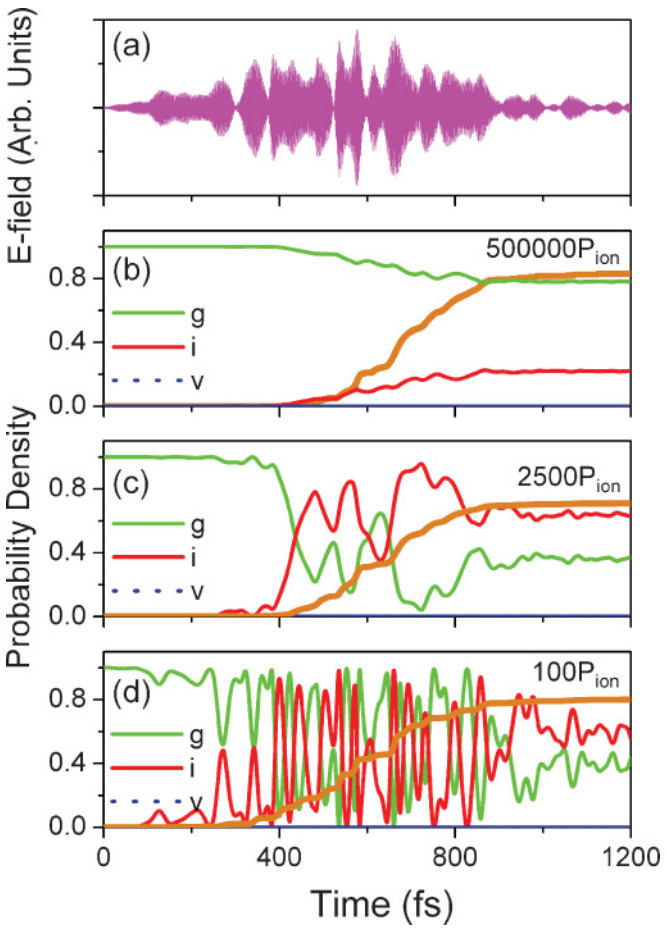

FIG. 6. (Color online) The time evolution (a) of the electric field of an FEL pulse and of the probability densities among the three levels for different U_{gi}: (b) 1.1×10^{-8}, (c) 3.0×10^{-7}, and (d) 1.1×10^{-5}. See the caption to Fig. 3 for other remarks.

power dependence of the resonance two-photon ionization of He through the $(2p)$-$(1s)$ resonance transition [16]. For the comparison, the horizontal axis U_{gi} used in displaying the results of simulation is transformed to the laser-intensity parameter I (in W/cm^2), as mentioned in the previous section. This can be simply done by substituting the value of the squared dipole transition moment matrix element $|T_{gi}|^2$ into Eq. (16). The value $|T_{gi}|^2 = 0.177$, which was calculated by using the accurate Hylleraas wave functions [27], has been adopted. The results, together with the experimental data, have been plotted in Fig. 7 as a function of I.

As shown in Fig. 7, the experimental data with the laser intensity centered at around $\sim 3 \times 10^{13}$ W/cm^2 correspond to the large U_{gi} regime where the slope of the ionization curve is $\sim$1. The experimental data indicated by the green circles agree well with the ionization curve of the simulation indicated by the red squares. Indeed, a linear least-squares fit to the experimental data has given a slope of 1.1 [16]. These observation rationalize the reason why the experimental ionization probability has a linear power dependence despite the fact that the He atom is ionized by absorbing two photons: As has been seen in Fig. 6(d), the probability density in the intermediate i state [the $(2p)$ ^1P state] saturates in the large U_{gi} regime because of the high-frequency Rabi oscillations

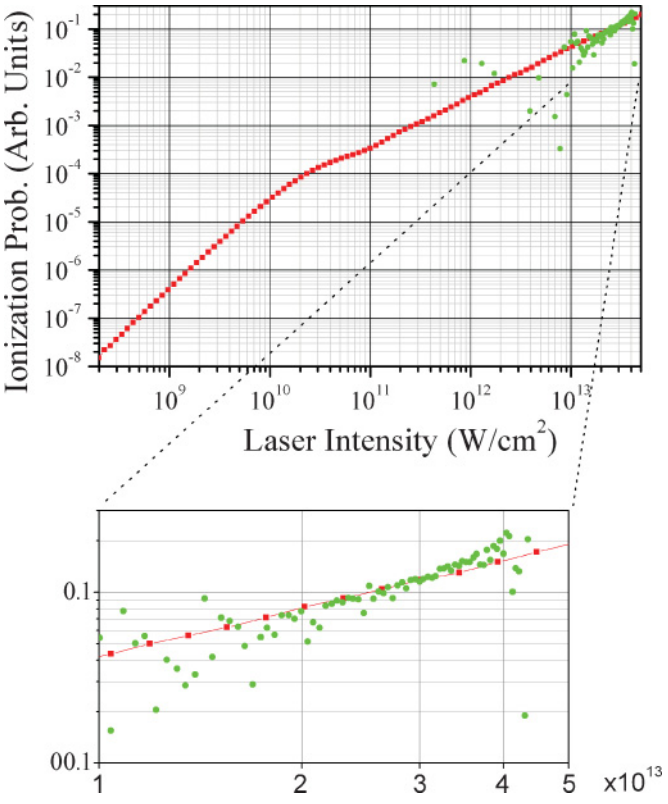

FIG. 7. (Color online) A comparison between the calculated and the experimental laser-power dependences (Ref. [16]) of the two-photon resonance ionization of He via the intermediate $(2p)\ ^1P$ state. The red (dark gray) squares and green (light gray) circles represent the calculated and experimental data, respectively.

between the g and i states. Therefore, the excitation from g to i does not have any dependence on I in this large U_{gi} regime, and the ionization probability thus has a linear intensity dependence through the one-way excitation from i to v.

IV. SUMMARY

The present study reports on the results of time-dependent numerical simulation for a light-coupled multilevel atom modeling the resonance two-photon ionization of an atom by strong EUV FEL pulses. The result for a single-mode Gaussian pulse of 100-fs duration shows that the ionization probabilities $P_{\rm ion}$ have characteristic dependences on the scaling parameter U_{gi}, namely, $P_{\rm ion} \propto (U_{gi})^n$, with n being equal to $\sim$2, less than 1, and $\sim$1 for the small, medium, and large U_{gi} regimes, respectively. The time evolution of the probability densities among the three states $|g\rangle$, $|i\rangle$, and $|v\rangle$, which represent, respectively, the ground, intermediate, and virtual states, has rationalized this nonmonotonous intensity dependence as being caused by different frequencies of Rabi oscillations between the $|g\rangle$ and $|i\rangle$ states for different U_{gi}. Further a numerical simulation employing the numerical data of SASE FEL pulses obtained from SIMPLEX has also been performed in order to examine effects of the multimode, non-Gaussian nature of SASE FEL pulses on the ionization probabilities. It shows that the above-mentioned nonmonotonous intensity dependence in the ionization probabilities persists for the SASE FEL pulses, except that the region of the ionization curve with a slope less than 1 in the medium U_{gi} regime is less clearly visible than the case for the single-mode Gaussian pulse. The Rabi oscillations between the ground and intermediate states also persist for the results by the SASE FEL pulses, although the time evolution of the probability densities and the ionization probabilities gets significantly modulated owing to the existence of other frequency components close to the main component of the resonance atomic transition.

The present result of the ionization probability curve obtained with the simulation showing the nonmonotonous intensity dependence has been compared with the experimental laser-intensity dependence for the two-photon resonance ionization of He measured recently by Sato *et al.* [16]. It is shown that the experimental data showing a linear intensity dependence correspond to the large U_{gi} regime of the simulation. The observed linear laser-intensity dependence has been thus rationalized as being caused by the strong Rabi oscillations between the ground $(1s)\ ^1S$ state and the intermediate resonance $(2p)\ ^1P$ state of He.

ACKNOWLEDGMENTS

The authors thank Dr. Takahiro Sato, Dr. Atsushi Iwasaki, Dr. Tomoya Okino, and Professor Kaoru Yamanouchi for providing us with the experimental data. T.S. gratefully acknowledges financial support from the Japan Society for the Promotion of Science (Grants-in-Aid for Scientific Research No. 23550025) and from the Nihon University Strategic Projects for Academic Research.

[1] T. Shintake *et al.*, Nat. Photonics **2**, 555 (2008).
[2] T. Shintake *et al.*, Phys. Rev. Spec. Top. Accel. Beams **12**, 070701 (2009).
[3] C. Cohen-Tannoudji, J. Dupont-Roc, and C. Crynberg, *Atom-Photon Interactions: Basic Processes and Applications* (Wiley-VCH, Weinheim, 2004), pp. 203–204.
[4] H. Wabnitz, A. R. B. de Castro, P. Gürtler, T. Laarmann, W. Laasch, J. Schulz, and T. Möller, Phys. Rev. Lett. **94**, 023001 (2005).
[5] R. Moshammer *et al.*, Phys. Rev. Lett. **98**, 203001 (2007).
[6] A. A. Sorokin, M. Wellhöfer, S. V. Bobashev, K. Tiedtke, and M. Richter, Phys. Rev. A **75**, 051402 (2007).
[7] A. A. Sorokin, S. V. Bobashev, T. Feigl, K. Tiedtke, H. Wabnitz, and M. Richter, Phys. Rev. Lett. **99**, 213002 (2007).
[8] M. Richter, M. Y. Amusia, S. V. Bobashev, T. Feigl, P. N. Juranic, M. Martins, A. A. Sorokin, and K. Tiedtke, Phys. Rev. Lett. **102**, 163002 (2009).
[9] M. Protopapas, C. H. Keitel, and P. L. Knight, Rep. Prog. Phys. **60**, 389 (1997).
[10] P. L. Knight, Opt. Commun. **22**, 173 (1977).

[11] P. Agostini, A. T. Georges, S. E. Wheatley, P. Lambropoulos, and M. D. Levenson, J. Phys. B **11**, 1733 (1978).
[12] H. Fukuzawa *et al*., J. Phys. B **43**, 111001 (2010).
[13] Y. Hikosaka *et al*., Phys. Rev. Lett. **105**, 133001 (2010).
[14] N. Miyauchi *et al*., J. Phys. B **44**, 071001 (2011); see also Europhys. News **42**, 14 (2011).
[15] M. Martins, M. Wellhöfer, A. A. Sorokin, M. Richter, K. Tiedtke, and W. Wurth, Phys. Rev. A **80**, 023411 (2009).
[16] T. Sato *et al*., J. Phys. B **44**, 161001 (2011).
[17] P. Lambropoulos, Adv. At. Mol. Phys. **12**, 87 (1976).
[18] K. Burnett, V. C. Reed, and P. L. Knight, J. Phys. B **26**, 561 (1993).
[19] J. Purvis, M. Dörr, M. Terao-Dunseath, C. J. Joachain, P. G. Burke, and C. J. Noble, Phys. Rev. Lett. **71**, 3943 (1993).
[20] C. McKenna and H. W. Van Der Hart, J. Phys. B **36**, 1627 (2003).
[21] C. McKenna and H. W. Van Der Hart, J. Phys. B **37**, 457 (2004).
[22] H. W. Van Der Hart and P. Bingham, J. Phys. B **38**, 207 (2005).
[23] L. Hamonou, H. W. Van Der Hart, K. M. Dunseath, and M. Terao-Dunseath, J. Phys. B **41**, 015603 (2008).
[24] I. Maruyama, T. Sako, and K. Yamanouchi, J. Phys. B **37**, 3919 (2004).
[25] K. Takahashi and K. Ikeda, J. Chem. Phys. **99**, 8680 (1993).
[26] T. Tanaka (private communication).
[27] B. Schiff, C. L. Pekeris, and Y. Accad, Phys. Rev. A **4**, 885 (1971).